npj | heritage science

Article

https://doi.org/10.1038/s40494-025-02125-8

Calcined clay's effect on the performance and mechanism of natural hydraulic lime grouting material

Chenhui Liu[1], Haitao Yan[1,2] ✉, Yanhong Li[1,2], Hongbin Zhang[2] & Yaxin Zhu[1]

The physical and mechanical properties of grouting material are critical indicators to assess its compatibility to earthen sites as a fissure repair material. This study activated the clay from Huangshan Archaeological Site by calcination to explore how calcined clay enhances the age performance of grouting material with various temperature and blending ratio. The results revealed calcined clay's effect of improving water retention and density of the slurry, reducing shrinkage and colour difference. The mechanical strength increased first and then decreased with rising calcination temperature, as clay's mineral activity was altered by phase transformation. At the microstructural level, stable minerals such as quartz and calcite provided a framework, while hydration products such as calcium silicate hydrate (CSH) and tetracalcium aluminate hydrate (C_4AH_{13}) interwove to form a denser pore structure. This modified grouting material with calcined clay demonstrates feasibility for earthen site restoration.

The central province of China, He'nan, contains various earthen archaeological sites with cultural significance in history, aesthetics and technology. These sites, including buildings and burials, were constructed from Neolithic Age for the purpose of production, life and defence[1]. Affected by many unfavourable factors such as composition materials[2], archaeological excavations and the occurrence environment[3], there are various types of fissures on the earthen sites. The developing fissure was leading to serious damage such as structural deformation, destabilisation or collapse[4,5]. Fissure grouting has become one of the most common and effective techniques for repairing fissures in earthen sites. The injected material sets and hardens into a grout concretion, which fills internal cavities and bonds loose soil, thereby helping to suppress further fissure development[6–9]. The appropriate selection of grouting materials is key to ensuring both compatibility with the surrounding substrate and long-term durability. Therefore, studying the selection of fissure grouting materials is essential for slowing the degradation process of earthen[10–12] sites and extending their preservation time.

In recent years, site soil and natural hydraulic lime (NHL) were used as base and improving materials correspondingly to enhance the properties of grouting material by changing the admixture dosage or binder[13,14]. Li[15], Sun[16] and Kalagri[17] found that NHL, when used as a fissure grouting material, offered advantages such as moderate strength, absence of soluble salts and good compatibility with the surrounding archaeological site soil. It performed well in improving the mechanical strength and durability of modified silty soils[18–20]. However, Song et al.[21] confirmed several drawbacks of NHL when applied to earthen site conservation, including low early-age strength, high shrinkage and noticeable colour differences[22,23], which limit its practical application. Based on conservation experience, Forster et al.[24] concluded that both the grade and dosage of NHL influence its durability under site conditions. Currently, researchers mainly attempt to overcome these limitations by incorporating active materials into the lime-based mix[25]. Wang[26] and Luo[27] studied the influence of nano-SiO_2 on the early physical properties and microstructure of NHL. Although nano-silicon dioxide was found to increase the quantity of hydration products and improve grout strength, its complex preparation process and unclear long-term durability have hindered widespread application. Zhang et al.[28] demonstrated that the addition of slag powder and silica fume can effectively improve the microstructure of NHL grout. However, due to their fine particle size and large specific surface area, these materials exhibited poor dispersion, strong autogenous shrinkage and a grey-black appearance, making them unsuitable for the repair of earthen archaeological sites. As a result, the search for active materials compatible with the substrate to modify or partially replace NHL has become a shared focus in current research.

Calcined clay is a commonly used active material[29,30]. It is inexpensive, readily available and derived from natural clay containing clay minerals such as kaolinite, montmorillonite and illite, as well as non-clay minerals including quartz and feldspar. Each type of clay mineral has a different optimal decomposition temperature, resulting in varied levels of pozzolanic activity following calcination[31]. Zhong et al.[32] conducted thermal activation

[1]He'nan Provincial Institute of Cultural Heritage and Archaeology, Zhengzhou, China. [2]Department of cultural heritage and museology, Fudan University, Shanghai, China. ✉e-mail: yanhaitaopku@163.com

experiments on natural clay under different temperatures and holding times. They found that calcination at 700°C for 3 hours produced the highest reactivity, allowing partial replacement of cement and resulting in approximately an 11% increase in the strength of blended mortar. Habert et al.[33] reported that the optimal decomposition temperatures for kaolinite, montmorillonite and illite were 700°C, 800°C and 850°C respectively, and that calcination temperature affected the effectiveness of these materials as cement substitutes. Wei et al.[34] examined the mineralogical composition and mechanical properties of blended cement mortars incorporating clays calcined at temperatures ranging from 600°C to 1100°C. They observed that pozzolanic activity initially increased and then declined as the calcination temperature rose. These findings suggest that calcined clay can enhance the activity of pozzolanic reaction of cement-based materials[35], although its potential to improve or partially replace NHL remains underexplored.

In this study, natural clay collected from the cultural layer of Yangshao at the Huangshan Archaeological Site was used as raw material. The clay was thermally activated at various calcination temperatures and subsequently ground before being blended with NHL to prepare fissure grouting materials. A control group consisting of NHL slurry without the addition of calcined clay was also prepared. The compatibility and applicability of the blended materials were evaluated by measuring their mass loss rate, linear shrinkage rate, P-wave velocity, age-related strength and visual appearance.

Fig. 1 | Sintering soil architectural remains at middle and late Yangshao archaeological site.

Fig. 2 | Wall remains of sintering soil architecture.

Furthermore, representative specimens were analysed using microscopic testing methods such as X-ray diffraction (XRD) and scanning electron microscopy (SEM) to investigate their mineralogical composition and microstructure. The study primarily examined the effects of calcination temperature and blending ratio of the calcined clay on the age performance of the grout concretion, with the aim of assessing the feasibility of partially replacing NHL with calcined clay and promoting its application in the fissure grouting repair of earthen archaeological remains.

Methods

Test material

The Huangshan Archaeological Site is located in Nanyang, Henan, China. Archaeological investigations have revealed large-scale architectural remains constructed from sintering soil with an orderly and layered spatial layout[36]. Existing studies have shown that the floors and walls of these structures were built and coated using natural clay, which was shaped and then fired under specific thermal conditions. The lower temperature threshold for this process was between 500°C and 600°C, while the upper limit ranged from 950°C to 1050°C[37,38], as illustrated in Figs. 1 and 2.

Natural hydraulic lime. The natural hydraulic lime used in this study was sourced from Shanghai Desaibao Building Materials Co., Ltd. Its mineralogical composition primarily consisted of the hydraulically reactive dicalcium silicate ($2CaO{\cdot}SiO_2$, abbreviated as C_2S), the air-hardening compound calcium hydroxide ($Ca(OH)_2$, abbreviated as CH), and partially calcined calcium carbonate ($CaCO_3$)[39,40].

Calcined clay. Calcined clay was prepared using raw material collected from the middle-to-late Yangshao cultural layer at the Huangshan Archaeological Site. The soil appeared greyish brown in colour. Its basic physical properties are shown in Table 1 and the oxide composition is listed in Table 2. According to the Chinese national standard – *the Standard for Geotechnical Testing Method* (GB/T 50123-2019), the tested soil was identified as low-plasticity clay. The soil was crushed using a soil pulveriser and then sieved to below 2 mm using a vibrating sieve for subsequent use. Informed by the firing temperatures of sintering soil remains at the site and by Grader et al.'s study[31] on the optimal calcination conditions for activating natural clay, the samples were fired in an SGM M15-14Y muffle furnace at 500°C, 700°C and 900°C for 2 hours, then allowed to cool naturally. The calcined samples were subsequently ground for 3 hours using a ball mill to obtain clays treated at different calcination temperatures (Fig. 3). The particle size distribution curves, mineralogical compositions and specific surface areas of the natural and calcined clays are presented in Figs. 4, 5 and 6 respectively.

The main mineralogical components of the natural clay included quartz, kaolinite and albite (Fig. 5). After calcination at 500°C, the mineral phases remained largely consistent with those of the raw material, although the intensity of the diffraction peaks associated with kaolinite was significantly reduced. This indicated that a portion of the kaolinite had transformed into amorphous metakaolin[41]. Following calcination at 700°C and 900°C, the diffraction peaks of kaolinite disappeared entirely. At this stage, the dominant mineral phases in samples T700 and T900 consisted of quartz, albite, aphthitalite and metakaolin. As the calcination temperature increased, the specific surface area of the calcined clay exhibited a general upward trend (Fig. 6). Compared to the untreated sample, specific surface area increased by 229.5%, 684.3% and 735.9% at 500°C, 700°C and 900°C respectively. In general, powder materials with larger specific surface areas tend to exhibit better dispersion when added to other matrices, thereby

Table 1 | The physical properties of natural clay

Materials	Natural moisture content	Natural density	Dry density	Porosity	Consistency index			Gradation characteristics	
					Liquid limit	Plastic limit	Plasticity index I_p	Coefficient of non-uniformity C_u	Coefficient of curvature C_c
	%	g·cm^{-3}	g·cm^{-3}	%	%	%			
Natural clay	8.56	1.80	1.66	26.5	19.2	8.22	10.98	6.42	0.86

Table 2 | Oxide composition of natural clay

Oxide	SiO_2	Al_2O_3	Fe_2O_3	K_2O	MgO	CaO	Na_2O	Otehr
Content	64.0	19.3	6.9	3.0	3.0	1.5	0.7	1.6

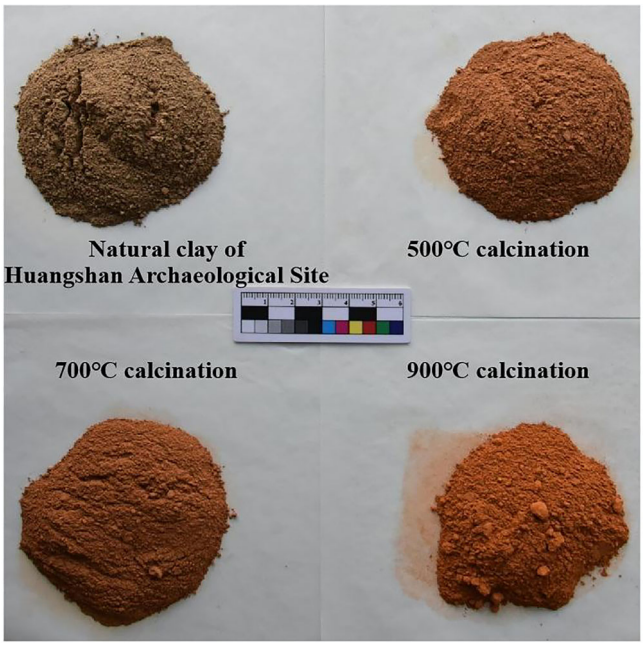

Fig. 3 | Site soil and clay with different calcination temperatures.

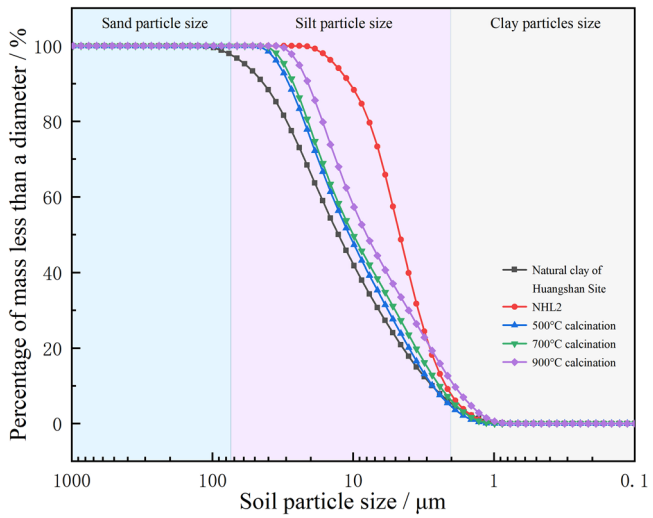

Fig. 4 | Particle size analysis of site soil and calcined clay.

enhancing their reinforcing effect. However, at 900°C, a dense vitreous phase formed on the surface of the clay particles[34], which hindered water penetration and consequently reduced the reactivity of the calcined clay.

Specimen preparation

To identify fissure grouting materials with good compatibility and applicability, 12 mix proportions were prepared using calcined clay at three temperatures (500°C, 700°C and 900°C) and four replacement ratios (5%, 10%, 20% and 30%). For example, T500-20% denotes a mixture comprising calcined clay fired at 500°C, added at 20% by mass and blended with 80% NHL. A control group using pure NHL without calcined clay was numbered as NHL2.

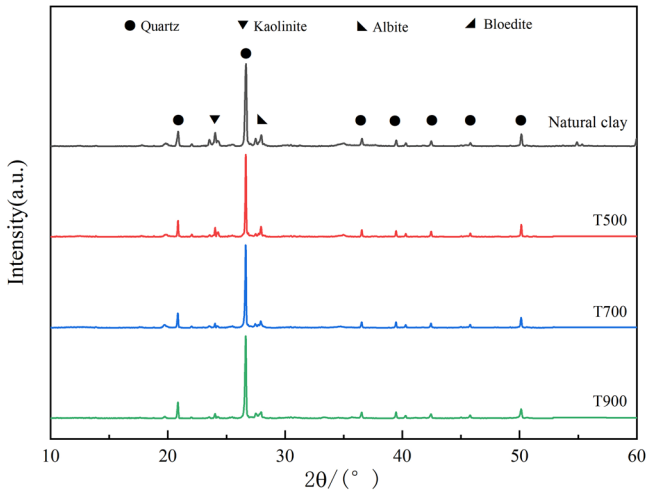

Fig. 5 | Natural clay and calcined clay XRD patterns.

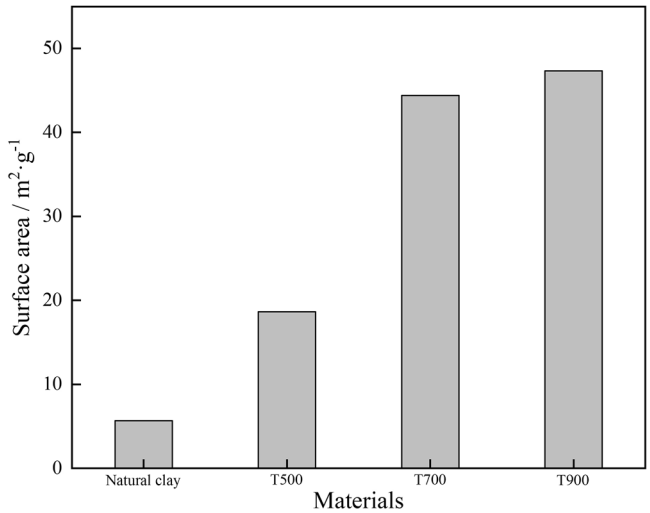

Fig. 6 | Natural clay and calcined clay specific surface area.

According to the mix promotions, the required amounts of calcined clay and NHL were weighed using a balance and dry-mixed in a container for 1 minute until homogeneous. Deionised water was then added at a water-cement ratio of 0.5. The grout was mixed using a JJ-5 cement mortar mixer at a speed of 450 r/min for 4 minutes until uniform. The initial fluidity of the grout was measured using the flow table method, and all samples showed a spread greater than 220 mm. The slurry was immediately poured into three-gang moulds (40 mm × 40 mm × 160 mm), filled in two layers. Each layer was compacted using a vibration table operating at 50 Hz with a 2 mm amplitude for 30 seconds to remove internal air bubbles. Excess slurry was levelled from the surface. The moulded specimens were then placed in a curing chamber in a controlled environment (25 ± 2°C, RH ≥ 90%). After 2 days of static curing, the hardened grout concretions were demoulded and returned to the curing chamber. Samples were tested at curing ages of 7, 14 and 28 days for physical property testing and microstructural analysis.

Physical property testing

For each mix design, the physical and mechanical properties of the grout concretion were tested at curing ages of 7, 14 and 28 days. Twelve specimens were prepared per mix. Three specimens were selected for repeated measurements at each curing age to determine the mass loss rate, linear shrinkage rate, P-wave velocity and colour difference. The remaining nine

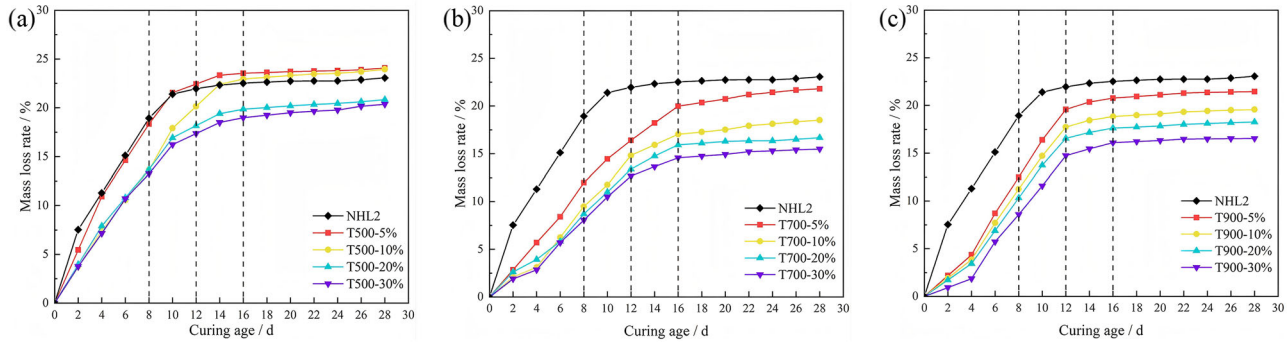

Fig. 7 | Effects of calcination temperature and replacement ratio of calcined clay on the mass loss rate. a T500, **b** T700, **c** T900.

specimens were used for testing compressive and flexural strength. The average value of three specimens taken as the final result.

Mass loss rate: The initial mass of the specimen at preparation was recorded as m_0. The mass at subsequent intervals was recorded as m_x, with measurements taken every two days. The mass loss rate during curing was calculated using Eq. (1), which reflects the rate of moisture loss.

Linear shrinkage rate: The initial length l_0 of the specimen was taken as 160 mm (the internal length of the mould). The specimen length l_x was measured every two days and the linear shrinkage rate was calculated using Eq. (2), which indicates the shrinkage behaviour of the grout concretion.

P-wave velocity: The P-wave velocity was measured using a ZBL-550 ultrasonic tester in accordance with *the Standard for Test Method of Basic Properties of Construction Mortar* (JGJ/T 70—2009). This parameter was used to evaluate the compactness and continuity of the specimens.

Mechanical properties: Compressive and flexural strengths at different curing ages were tested using a WDW-300 universal testing machine, following the procedures outlined in *the Test Method of Cement Mortar Strength (ISO Method)* (GB/T 17671—2021).

Colour difference analysis: The surface chromatic parameters of the specimens were measured using a CR-400 colourimeter in accordance with *the Uniform Colour Space and Colour Difference Formula* (GB/T 7921–2008).

$$\omega_m = \frac{m_0 - m_x}{m_0} \times 100\% \quad (1)$$

$$\omega_l = \frac{l_0 - l_x}{l_0} \times 100\% \quad (2)$$

Mineralogical and morphological analysis

The properties of inorganic cementitious materials such as NHL largely depend on the mineralogical composition and pore structure developed during the hardening process. By analysing the formation of hydration and carbonation products within the grout concretion and observing the changes in microstructure, this study aimed to elucidate the mechanisms by which calcined clay improves the performance of NHL slurry.

XRD: Representative grout specimens were selected for analysis. Residual fragments from the mechanical strength tests were crushed into powder and passed through a sieve. X-ray diffraction analysis was performed using a German-manufactured Bruker S2 Range diffractometer. The testing parameters were as follows: Cu target K radiation with a wavelength of 1.5418 Å, tube voltage of 40 kV, current of 40 mA, scanning range from 10° to 60°, and a step size of 0.02 mm.

SEM-EDS: Representative grout specimens were selected and the fracture surfaces were examined using an FEI QUANTA 650 environmental SEM equipped with an EDAX APOLLO-X EDS system. The measurement was conducted in high vacuum mode at an accelerating voltage of 25 kV, with both secondary electron and backscattered electron imaging. The EDS scan time was 30 seconds and the working distance was set to 10 mm.

Results

Mass loss rate

Figure 7 illustrates the variation in mass loss rate over the 28-day curing period for grout concretion made from calcined clay–NHL slurry under different calcination temperatures and replacement ratios. The mass loss rate of grout concretion specimens followed a similar trend across all groups. It increased linearly at first, then gradually slowed, and eventually stabilised. The most significant increase in mass loss occurred within the first 16 days of curing. At 8, 12 and 16 days, under the same replacement ratio, the mass loss rate followed the order T500 > T900 > T700. The T700-30% group exhibited the lowest mass loss rate, indicating the least moisture evaporation and the best water retention, with reductions of approximately 57.4% at 8 d and 35.3% at 16 d compared to the control group (NHL2). At 28 days, the mass loss rates of the T500, T700 and T900 specimens ranged between 20.4–24.1%, 15.5–21.8% and 16.5–21.4% respectively. Under the same calcination temperature, increasing the replacement ratio of calcined clay led to a gradual reduction in the mass loss rate. For example, at 700°C, the mass loss rate of the T700-30% group was 15.5%, representing reductions of approximately 28.9%, 16.4% and 7.1% compared to the 5%, 10% and 20% groups respectively, and a decrease of 32.7% compared to the control group. Previous studies have shown that the early stage of NHL hardening is dominated by hydration reactions, which proceed relatively quickly. Rapid moisture loss is detrimental to both the continuation of hydration and the development of carbonation. Increasing the proportion of calcined clay can significantly reduce and slow down moisture loss, thereby enhancing the water-retention capacity of the slurry and helping to maintain a stable internal moisture environment within the hardened grout concretion.

Linear shrinkage rate

The dehydration and solidification process of the slurry is accompanied by internal autogenous shrinkage, carbonation shrinkage and drying shrinkage. During the early stage of curing, more than 67.3% of the total shrinkage observed at 28 days occurred before demoulding, within the first 2 days. Figure 8 presents the variation in linear shrinkage rate of the grout concretion specimens at 28 days of curing.

At 28 days of curing, the linear shrinkage rates of the T500, T700 and T900 grout concretion specimens ranged from 2.4% to 2.8%, 1.4% to 1.7% and 1.1% to 1.4% respectively. The lowest shrinkage was recorded in the specimens calcined at 900°C. In comparison, the control group (NHL2) exhibited a shrinkage rate of 2.0%. At the same calcination temperature, the linear shrinkage rate decreased progressively with increasing calcined clay content. When the replacement ratio increased from 5% to 30%, the shrinkage rate of T500, T700 and T900 decreased by approximately 25.7%, 32.8% and 29.8% respectively. These findings indicate that the addition of calcined clay helps to reduce the shrinkage of grout concretions. The effect is inversely related to both the calcination temperature and the replacement ratio. A lower shrinkage rate during the hardening process is beneficial for effective fissure filling and for minimising surface shrinkage cracking. This

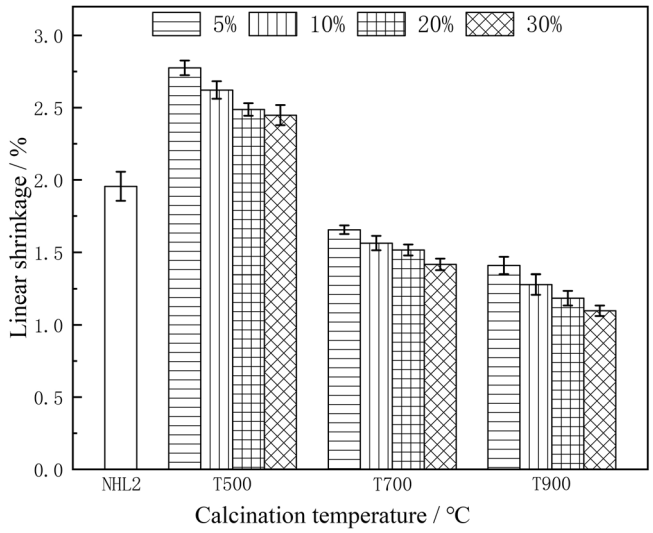

Fig. 8 | Effects of calcination temperature and replacement ratio of calcined clay on the linear shrinkage rate of grout concretion at 28 days.

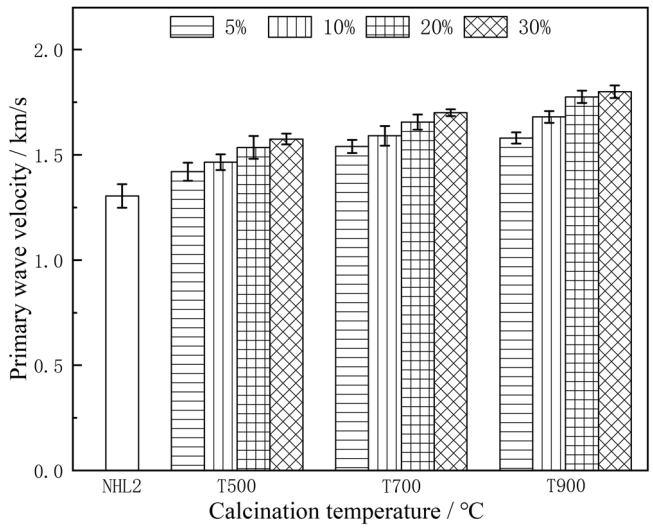

Fig. 9 | Effects of calcination temperature and dosage of natural clay on the P-wave velocity at 28 d.

in turn prevents rainwater ingress and helps maintain the continuity of the slurry–soil interface, thereby improving the overall integrity between the new grout and the existing earthen substrate.

P-wave velocity

Figure 9 shows the variation in P-wave velocity of grout concretion specimens at 28 days of curing, with respect to calcined clay temperature and replacement ratio. Under the same replacement ratio, the P-wave velocity of grout concretion specimens increased progressively with rising calcination temperature. The velocity ranges for T500, T700 and T900 specimens were 1.42–1.58 km/s, 1.54–1.70 km/s and 1.58–1.78 km/s respectively, all of which were higher than that of the control group (NHL2), which recorded 1.30 km/s. Taking a replacement ratio of 30% as an example, when the calcination temperature was raised from 500°C to 700°C and 900°C, the P-wave velocity increased by approximately 7.6% and 13.9% respectively, representing an overall improvement of about 20.6% compared to specimens without calcined clay. At any given calcination temperature, the P-wave velocity increased with higher replacement ratios of calcined clay, following a consistent trend. These results indicate that increasing both the calcination temperature and the replacement ratio of calcined clay leads to enhanced P-wave velocity in the grout concretion. However, the extent of improvement varied depending on the specific temperature and dosage. Higher P-wave velocity values reflect greater internal compactness and continuity, which are favourable for enhancing the physical and mechanical performance of the specimens.

Compressive strength

The relationship between compressive strength and curing age for grout concretions prepared with different calcination temperatures and replacement ratios is shown in Fig. 10. The compressive strength increased rapidly with curing time, with over 75% of the 28-day strength achieved within the first 14 days. This indicates that the hardening process progressed quickly during the early curing stage, highlighting the importance of maintaining internal moisture stability during this period. With increasing calcination temperature, the age-related compressive strength showed an overall trend of first increasing and then decreasing, following the order T700 > T900 > T500 > NHL2. For instance, at a 20% replacement ratio, the 28-day compressive strength of the T700 specimen reached 2.97 MPa, which was approximately 22.2% and 3.1% higher than that of the T500 and T900 specimens respectively. At all calcination temperatures, the compressive strength increased with higher calcined clay content, although the degree of increase varied. For specimens calcined at 700°C, increasing the replacement ratio from 5% to 10%, 20% and 30% resulted in strength

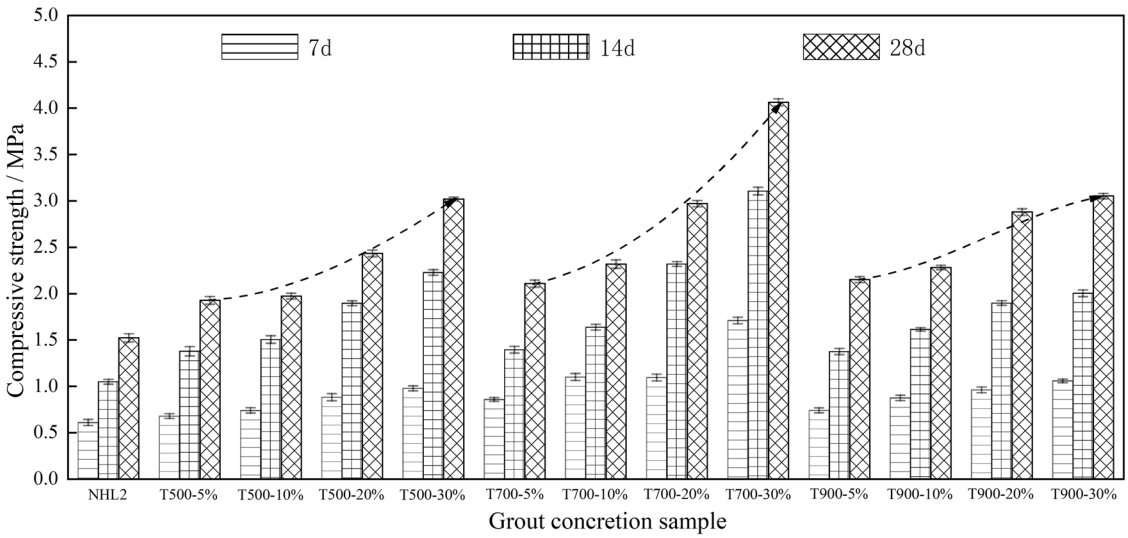

Fig. 10 | Effects of calcination temperature and replacement ratio of calcined clay on the compressive strength of grout concretion with curing age.

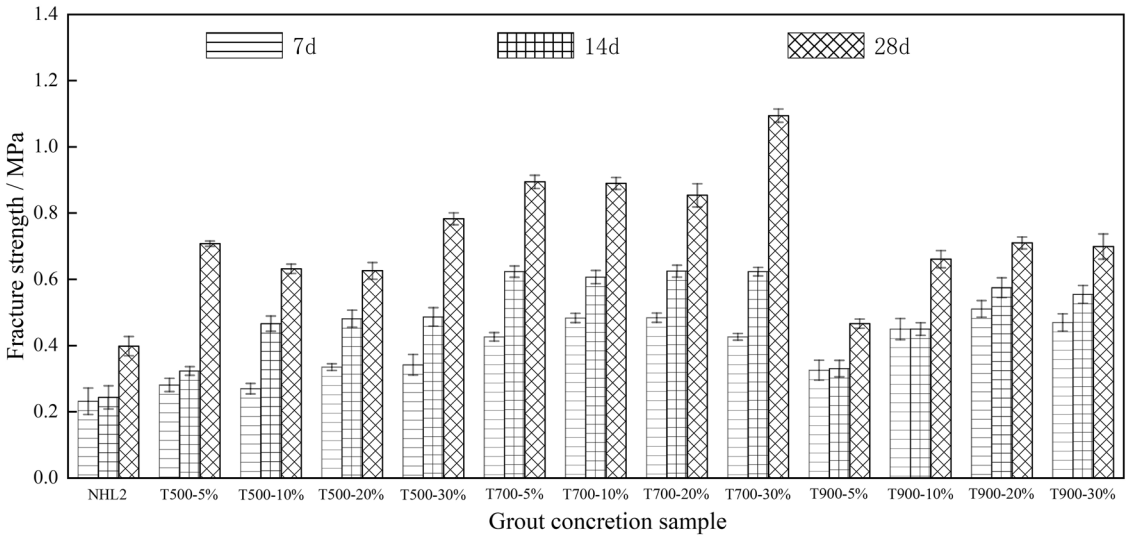

Fig. 11 | Effects of calcination temperature and replacement ratio of calcined clay on the flexural strength of grout concretion with curing age.

Table 3 | Chromaticity values and colour differences of grout concretion specimens.

Sample	T500					T700					T900				
	L^*	a^*	b^*	ΔE	Colour	L^*	a^*	b^*	ΔE	Colour	L^*	a^*	b^*	ΔE	Colour
5%	75.47	2.16	10.51	17.5		74.84	2.81	12.25	15.6		75.72	3.42	14.54	14.4	
10%	73.13	2.27	11.56	15.4		74.73	4.08	14.64	13.4		73.59	5.45	17.75	10.2	
20%	67.23	5.84	18.61	5.9		72.75	6.25	15.54	11.5		72.40	7.20	18.45	8.5	
30%	64.15	7.96	22.72	2.0		68.20	8.65	23.49	2.4		68.27	8.15	20.98	3.6	

improvements of 10.0%, 40.8% and 92.4% respectively. In comparison, the strength increments from 5% to 30% for T500 and T900 were relatively smaller, at 56.5% and 41.9% respectively. This behaviour can be attributed to the influence of calcination temperature on the pozzolanic reactivity of the calcined clay. At 700°C, the reactivity of the clay improved, promoting the hydration process and increasing the formation of hydration products. Moreover, the addition of calcined clay reduced the shrinkage of the specimens, helping to suppress the formation of fissures and defects, thereby enhancing mechanical performance. In contrast, calcination at 900°C inhibited hydration reactions and reduced the amount of hydration products, resulting in a decline in compressive strength.

Flexural strength

The influence of calcination temperature and replacement ratio on the age-related flexural strength of grout concretion is shown in Fig. 11. The variation in flexural strength followed a trend similar to that of compressive strength. As the calcination temperature increased, the flexural strength initially increased and then decreased, following the order T700 > T500 > T900 > NHL2. Among all groups, the T700-30% specimens exhibited the highest flexural strength. At any given calcination temperature, the flexural strength increased with higher replacement ratios of calcined clay. For example, at a calcination temperature of 700°C, when the replacement ratio increased from 5% to 30%, the 28-day flexural strength reached a maximum of 1.09 MPa, with an increase of 22.4%. For T500 and T900, the corresponding increases were 10.6% and 19.9% respectively. A comparative analysis of compressive and flexural strengths revealed that, while both improved with higher calcination temperature and replacement ratio, the increase in flexural strength was significantly smaller than that in compressive strength. This suggests that the brittleness of the specimens increased, increasing the risk of abrupt brittle failure under mechanical stress[42]. In line with the principle of mechanical compatibility between the grout concretion and the archaeological substrate, the addition of calcined clay at appropriate calcination temperatures and replacement ratios can effectively improve the strength compatibility between the two.

Colour difference analysis

In addition to meeting mechanical compatibility requirements, the applicability of fissure grouting materials must also be considered. Specifically, they should achieve visual consistency at a distance while remaining distinguishable at close range and exhibit a chromaticity that harmonises with the original archaeological substrate. The CIE $L^*a^*b^*$ colour model comprises three parameters: L^* for lightness, a^* for the red–green component and b^* for the yellow–blue component. For each grout concretion specimen with different mix proportions, the L^*, a^* and b^* values were measured. The colour difference (ΔE) between the specimens and the sintering soil wall remains ($L^* = 65.81$, $a^* = 8.54$, $b^* = 23.61$) was then calculated according to the CIE $L^*a^*b^*$ colour space method using Eq. (3)[43].

$$\Delta E = \sqrt{(\Delta L^*)^2 + (\Delta a^*)^2 + (\Delta b^*)^2} \tag{3}$$

where ΔL^*, Δa^* and Δb^* represent the differences in lightness, red–green component and yellow–blue component respectively between the grout concretion and the sintering soil wall remains. Table 3 presents the chromatic values and colour differences of the grout concretion specimens.

At any given calcination temperature, an increase in the replacement ratio of calcined clay led to a decrease in L^* value, indicating reduced lightness. Meanwhile, both the a^* and b^* values increased, suggesting

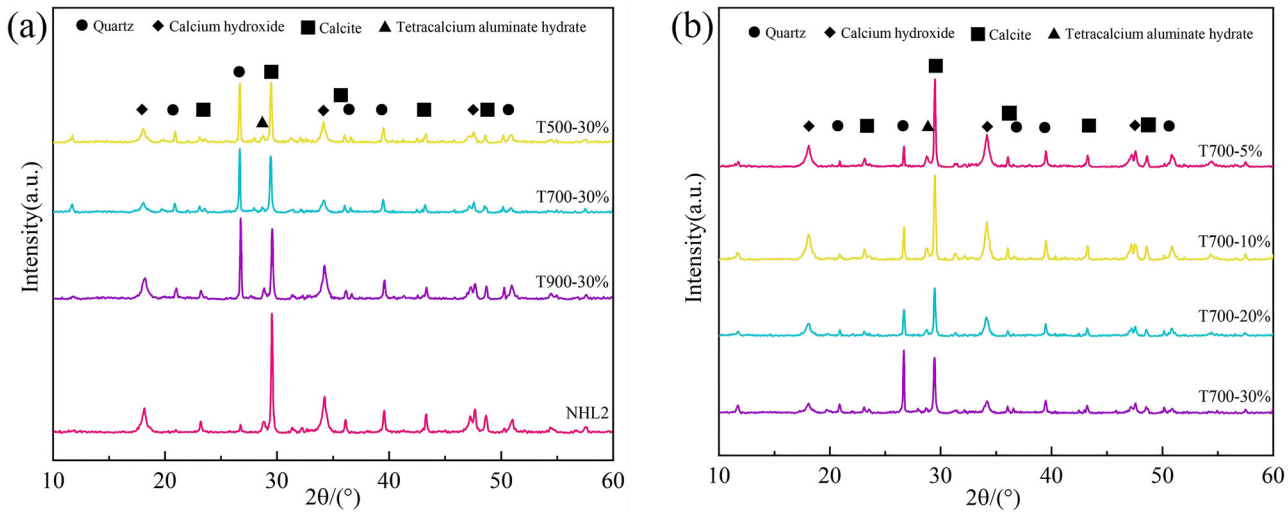

Fig. 12 | XRD patterns of grout concretion specimens at 28 days. a Different calcination temperatures and control group, **b** Different replacement ratio.

enhanced red saturation and a shift towards a yellow hue. As a result, the overall colour of the grout concretion became increasingly similar to that of the architectural remains made of sintering soil. With rising calcination temperature, the a^* value gradually increased, indicating a strengthening of the red tone in the specimens. Among all groups, the a^* value of the specimens calcined at 700°C was the closest to that of the original archaeological sites soil.

Comprehensive evaluation of the colour difference indicated that ΔE decreased progressively with increasing replacement ratio of calcined clay. According to human visual sensitivity to colour differences[44], when the replacement ratio reached 30%, the ΔE value ranged from 2.0 to 3.6, corresponding to a level of difference that was either perceptible or distinguishable. Based on field conservation experience, it is generally accepted that the closer the appearance of the grout concretion is to the original material in colour, the less post-repair colour blending is required. Ideally, the material should be recognisable yet visually coherent with the heritage structure. In contrast, the control group (NHL2) exhibited a grey appearance ($L^* = 78.98$, $a^* = 1.04$, $b^* = 7.95$), showing a much greater colour discrepancy compared to the sintering soil architectural remains. Taking into account both colour difference and on-site performance, the T700-30% group was considered most suitable for the fissure grouting repair of sintering soil architectural remains at the Huangshan Archaeological Site.

Mineralogical composition

During the hydration and hardening process of NHL, the hydraulic phase dicalcium silicate (C_2S) reacts with water to form calcium silicate hydrate ($CaO{\cdot}SiO_2{\cdot}H_2O$, abbreviated as CSH) and calcium hydroxide (CH). Concurrently, both CSH and CH undergo carbonation reactions. Due to the weak crystallinity of CSH, its diffraction intensity is relatively low. Therefore, CH and calcium carbonate ($CaCO_3$) were used as representative phases to investigate the effects of calcination temperature and replacement ratio on the hardening process of NHL. Figure 12 shows the XRD patterns of the 28-day grout concretion specimens prepared from NHL slurry modified with calcined clay.

As shown in Fig. 12a and b, compared with the control group (NHL2), the addition of calcined clay led to a significant increase in the diffraction peak intensity of quartz in the grout concretion. $CaCO_3$ and CH remained the main mineralogical phases, though their diffraction intensities exhibited varying changes. With increasing calcination temperature, the diffraction peak intensity of CH first decreased and then increased. When the calcination temperature rose from 500°C to 700°C, the consumption of CH increased, although the diffraction intensity of $CaCO_3$ showed no significant change. At 900°C, the CH consumption was reduced and the diffraction intensity of $CaCO_3$ decreased. According to previous studies by Zhong[32], Wei[45] and other researchers on the thermal activation of natural clay, kaolinite within the raw material undergoes a dehydroxylation reaction between 514.6°C and 600°C to form semi-crystalline metakaolin[46]. When blended into NHL, this metakaolin exhibits high reactivity. Furthermore, the increased specific surface area of the clay particles improves their dispersion. The highly active quartz and aluminium oxide within the calcined clay react pozzolanically with Ca^{2+} and OH^- ions released from CH in the presence of water, forming hydration products such as calcium silicate hydrate (CSH) and tetracalcium aluminate hydrate (C_4AH_{13}). The corresponding hydration and hardening processes are illustrated in Eqs. (4) to (6), with enhanced reinforcement effects. Since the carbonation of CH by CO_2 is relatively slow, the change in calcite diffraction peak intensity remained limited. When the calcination temperature increased to 850-900°C, firing of kaolinite occurred. Although the specific surface area further increased, a dense vitreous layer formed on the surface of the clay particles, preventing water penetration. At the same time, the metakaolin decomposed into amorphous silicon dioxide (SiO_2) and aluminium oxide (Al_2O_3), resulting in a gradual decline in the reactivity of the calcined clay. This led to reduced formation of hydration and carbonation products, which was unfavourable for improving the mechanical performance of the grout concretion.

$$Al_2O_3 \cdot 2SiO_2 + 3Ca(OH)_2 + 6H_2O \rightarrow 2Cao \cdot Al_2O_3 \cdot SiO_2 \cdot 8H_2O + CaO - SiO_2 - H_2O \quad (4)$$

$$Al_2O_3 \cdot 2SiO_2 + 6Ca(OH)_2 + 9H_2O \rightarrow 4CaO \cdot Al_2O_3 \cdot 13H_2O + 2CaO - SiO_2 - H_2O \quad (5)$$

$$Ca(OH)_2 + CO_2 \rightarrow CaCO_3 + H_2O \quad (6)$$

At different calcination temperatures, the mineralogical composition of the grout concretion exhibited similar trends with increasing replacement ratios of calcined clay. As shown in Fig. 12b, taking 700°C as an example, the diffraction peak intensity of CH gradually decreased with higher calcined clay content, while the intensity of unreacted quartz increased significantly. This unreacted quartz influences the internal pore structure of the grout concretion, thereby affecting its mechanical performance.

Microstructural characterisation

SEM was used to observe the influence of calcination temperature and replacement ratio of natural clay on the microstructure and pore structure of NHL slurry. The results are presented in Fig. 13. The panels (a) to (d), combined with EDS results for Ca/Si atomic ratio determination, showed that crystalline hydration products such as CSH and C_4AH_{13} were present in specimens without calcined clay. However, the structure was relatively

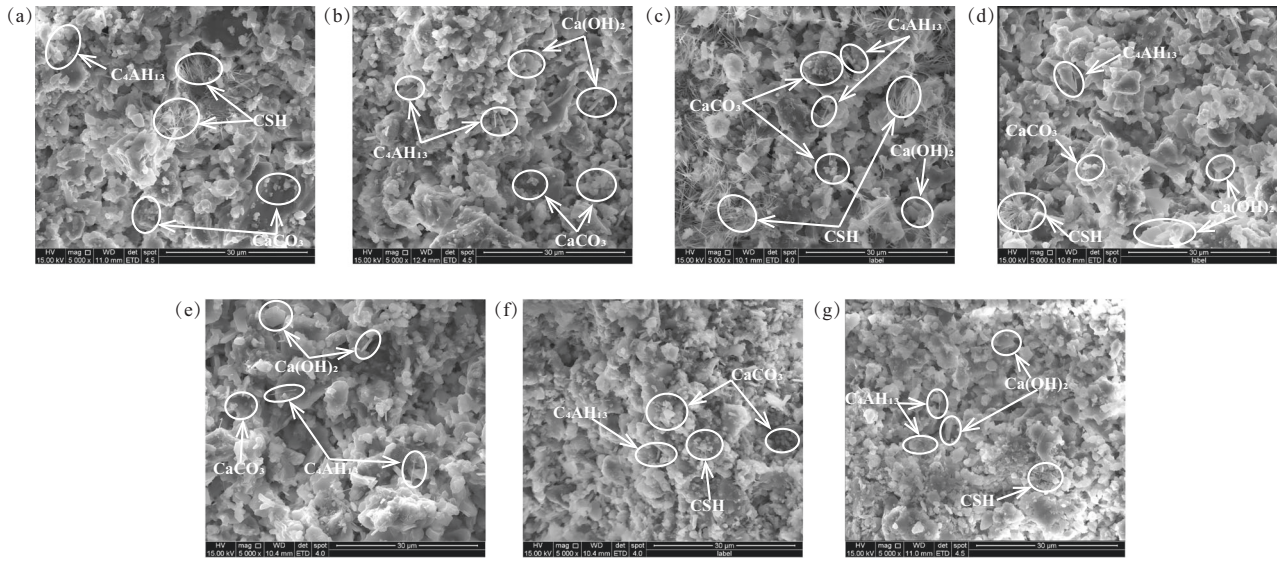

Fig. 13 | SEM images of grout concretion specimens at 28 days. a NHL2, **b** T500–30%, **c** T700–30%, **d** T900–30%, **e** T700–5%, **f** T700–10%, **g** T700–20%.

loose and contained numerous pores. After the addition of calcined clay, the microstructure of the grout concretion became more compact. Stable minerals such as quartz and calcite acted as a skeletal framework within the matrix. Plate-like CH and granular $CaCO_3$ were deposited on the surfaces of clay particles and within the pore spaces, while fibrous CSH and needle-like C_4AH_{13} connected the clay particles to form a stable microstructure, improving the overall physical performance of the material. With increasing calcination temperature of the natural clay, the amount of needle-like hydration products increased and the interwoven particles filled the pore spaces more effectively. However, when the calcination temperature reached 900°C, the amount of hydration products decreased noticeably, while the CH content increased rather than declined. This indicated that the hydration process was inhibited, and the carbonation process remained slow, offering limited benefit to the mechanical strength. As shown in panels (e) to (g) in Fig. 13, when the calcination temperature was 700°C and the replacement ratio was 5%, the CSH and $CaCO_3$ products were relatively dispersed. With higher replacement ratios, the relative content of CH decreased significantly, and hydration products such as CSH and C_4AH_{13} formed a denser network structure. The quantity of unreacted minerals such as quartz and calcite also increased, gradually filling the pores. As a result, both the number and size of pores decreased, leading to a denser internal structure and reduced shrinkage in the slurry. Based on these findings, it is concluded that increasing the replacement ratio of calcined clay can effectively reshape the internal pore structure of the grout concretion.

Discussion

The incorporation of calcined clay was found to improve the compatibility, age properties and microstructure of NHL. The extent of improvement was influenced by both the calcination temperature and the replacement ratio. As the calcination temperature and replacement ratio increased, the mass loss rate and linear shrinkage rate of the grout concretion decreased, while its compactness improved. However, both compressive and flexural strengths increased initially and then declined with rising calcination temperature. Compared with NHL slurry without calcined clay, the T700-30% mixture demonstrated better water retention, lower shrinkage and greater compactness. It also fulfilled the mechanical and colour compatibility requirements for the repair of sintering soil heritage sites. At the microstructural level, stable minerals such as quartz and calcite provided a supporting framework, while hydration products such as CSH and C_4AH_{13} formed a denser cementitious microstructure. As the replacement ratio of calcined clay increased, the content of stable minerals and hydration products also increased, contributing to a further reduction in pore number and size.

Compared with existing research, the calcination temperature is a key factor affecting the pozzolanic reactivity of natural clay. When the calcination temperature reached 700°C, the specific surface area of the clay particles increased significantly and the dehydroxylation of kaolinite led to the formation of highly active metakaolin. This resulted in a substantial increase in the content of hydration and carbonation products within the grout concretion. However, further increasing the temperature to 900°C led to firing of kaolinite, decomposition of metakaolin and illite, and a reduction in specific surface area. These effects reduced the reactivity of the calcined clay, inhibited the formation of hydration products and ultimately caused a decline in mechanical performance. Therefore, for fissure repair of different types of archaeological substrates, adjusting the calcination temperature and replacement ratio of natural clay can help to meet specific requirements for mechanical strength and visual compatibility. On-site testing is recommended to determine the most suitable grout mix proportion for each case.

At present, research on calcined clay-modified NHL grouting materials remains largely qualitative. Further comprehensive and quantitative studies are required to clarify the underlying reinforcement mechanisms. In addition, it is necessary to investigate the deterioration patterns and degradation mechanisms between the grout and archaeological soil under various adverse environmental conditions to support the selection of the most durable and compatible grouting formulations for site application.

Data availability

No datasets were generated or analysed during the current study.

Received: 9 April 2025; Accepted: 16 October 2025;
Published online: 17 November 2025

References

1. Sun, M. L. & Dou, Z. C. Research progress and trend of earthen sites conservation in China: quantitative analysis based on literature. *Sci. Conserv. Archaeol.* **04**, 143–153 (2024).
2. Liu, H. Y. et al. Weathering types, mechanism and protection of rammed earth sites: progress and prospect. *Earth Sci.* **50**, 2284–2297 (2025).
3. Yue, J. W., Huang, X. J., Zhao, L. M. & Wang, Z. F. Micro-scale analysis of dry-shrinkage deterioration mechanism of Zhouqiao earthen soil. *Adv. Eng. Sci.* **54**, 109–119 (2022).
4. Lu, J. C. & Zhao, H. Y. Research on characteristics of diseases of Kizilgaha Beacon Tower based on quantitative analysis. *Sci. Conserv. Archaeol.* **01**, 103–109 (2021).

5. Yan, H. T., Zhou, S. L. & Tang, J. Investigation into damages threatening foundations of houses made of baked terracotta at Dahe Village site and analysis of damage causes. *Huaxia Archaeol.* **06**, 108–115 (2019).
6. Cui, K. et al. Comparison of bond performance between grouting slurry and soil interface in soil sites and durability in arid environment. *J. Jilin Univ. (Eng. Technol. Ed.)* . **10**, 2856–2868 (2023).
7. Cui, K. et al. Influence of grouting mode on the adhesion property of slurry-soil interface for fissure reinforcement of earthen sites. *Rock. Soil Mech.* **42**, 1501–1511 (2021).
8. Varum, H., Parisi, F., Tarque, N. & Silveira, D. Structural Characterization and Seismic Retrofitting of Adobe Constructions (2021).
9. Yue, J. W. et al. Strength characteristics and mechanism of modified imitation ruins soil of Qicheng site with glutinous rice slurry. *J. Civ. Environ. Eng.* **44**, 195–204 (2022).
10. Xu, S. Q. & Ma, Q. L. A state of the art review on natural hydraulic lime based mortars for restoration of historic buildings. *Res. Conserv. Cave Temples Earthen Sites.* **1**, 81–92 (2022).
11. Wang, J. Y. et al. Research progress on hydraulic lime for architectural heritage restoration. *Mater. Rep.* **39**, 24100053 (2025).
12. Lanas, J., Pérez Bernal, J. L., Bello, M. A. & Galindo, J. I. A. Mechanical properties of natural hydraulic lime-based mortars. *Cem. Concr. Res.* **34**, 2191–2201 (2004).
13. Moropoulou, A. et al. Strength development and lime reaction in mortars for repairing historic masonries. *Cem. Concr. Compos.* **27**, 289–294 (2005).
14. Ijaz, N. et al. Global insights into micro-macro mechanisms and environmental implications of limestone calcined clay cement (LC3) for sustainable construction applications. *Sci. Total Environ.* **907**, 167794 (2023).
15. Li, L., Zhao, L. Y. & Li, Z. X. Study on the physical and mechanical properties of several lime materials in ancient Chinese architecture. *Sci. Conserv. Archaeol.* **26**, 74–84 (2014).
16. Sun, Y. Z. Study on the performance of hydraulic lime modified soil materials. *Sci. Conserv. Archaeol.* **27**, 27–30 (2015).
17. Kalagri, A., Miltiadou-fezans, A. & Vintzileou, E. Design and evaluation of hydraulic lime grouts for the strengthening of stone masonry historic structures. *Mater. Struct.* **43**, 1135–1146 (2010).
18. Cizer, Z., Balen, K. V. & Gemert, D. V. Competition between hydration and carbonation in hydraulic lime and lime-pozzolana mortars. *Adv. Mater. Res.* **1**, 241–247 (2010).
19. Wei, X. H. et al. Effect of TEA-DEC compounding on the early hardening process of natural hydraulic lime. *J. Chongqing Univ.* **47**, 141–151 (2024).
20. Elsen, J., Jackson, M. D. & Ruiz-Agudo, E. Historic concrete science: opus caementicium to “Natural Cements”. *Elements* **18**, 301–307 (2022).
21. Song, Z., Lu, Z. & Lai, Z. Mechanical and durability performance improvement of natural hydraulic lime-based mortars by lithium silicate solution. *Materials* **13**, 5292–5305 (2020).
22. Wang, Y. et al. Research on microstructure and porosity calculation of rammed soil modified by lime-based materials: the case of rammed earth of Pingyao city wall, a world heritage site. *Environ. Earth Sci.* https://doi.org/10.1007/s12665-024-11944-0 (2024).
23. Xu, S. Q., Wang, L. L., Ma, Q. L. & Wang, J. L. Hydration of natural hydraulic lime pastes under different conditions of carbonation. *Sci. Conserv. Archaeol.* **29**, 1–8 (2017).
24. Forster, A. M. & Carter, K. A framework for specifying natural hydraulic lime mortars for masonry construction. *Struct. Surv.* **29**, 373–396 (2015).
25. Zhang, B. et al. Effect of graphene oxide on hydration and mchanical properties of natural hydraulic lime. *Bullftin Chin. Ceram. Soc.* **43**, 2640–2648 (2024).
26. Wang, Y., Fang, G. X., Zhang, D. M. & Wang, W. C. Effect of nano-silica on gelling properties of hydraulic lime. *Inorg. Chem. Ind.* **55**, 75–80 (2023).
27. Luo, K. et al. Influence of nano-SiO_2 and carbonation on the performance of natural hydraulic lime mortars. *Constr. Build. Mater.* **235**, 117411 (2020).
28. Zhang, Y. B. et al. Study on the hydration and microstructure of B and B/Na ion-doped natural hydraulic lime composed with silica fume/fly ash. *Sustainability* **14**, 10484–10484 (2022).
29. Brigatti, M. F. Structure and mineralogy of clay minerals. *Dev. Clay Sci.* **10**, 19–86 (2013).
30. Meddah, M. S. et al. Synergistic effect of combining low kaolinite grade calcined clay with conventional cementitious materials. *Innovative Infrastructure Solutions*. **9** https://doi.org/10.1007/s41062-024-01441-5 (2024).
31. Grader, G. S., Shter, G. E., Shvarzman, A. & Kovler, K. The effect of dihydroxylation / amorphization degree on pozzolanic activity of kaolinite. *Cem. Concr. Res.* **33**, 405–416 (2003).
32. Zhong, W. L. & Fan, L. F. Investigation on pozzolanic activity of natural clay. *Bull. Chin. Ceram. Soc.* **39**, 2196–2203 (2020).
33. Habert, G. et al. M. Clay content of argillites: influence on cement based mortars. *Appl. Clay Sci.* **43**, 322–330 (2009).
34. Wei, C. D. et al. Phase transformation for calcined coal measures kaolinite. *J. Chin. Ceram. Soc.* **33**, 77–81 (2005).
35. Siddique, R. & Klaus, J. Influence of metakaolin on the properties of mortar and concrete: a review. *Appl. Clay Sci.* **43**, 392–400 (2009).
36. Ma, J. C., Yan, H. T. & Wang, F. J. The neolithic site of Huangshan in Nanyang city, Henan. *Archaeology* **10**, 3–28 (2022).
37. Li, N. S., Wang, J. H. & Mao, Z. W. A preliminary study on the construction technology of red clay row houses at the site of Weichi Temple in Mengcheng County, Anhui Province. *Archaeology* **10**, 76–82 (2005).
38. Li, X. et al. Determination of the thermal temperatures of burnt clay at Sujiacun site based on magnetic susceptibility. *Sci. Conserv. Archaeol.* **34**, 63–70 (2022).
39. Maria, A., Asterios, B. & Meletis, K. Mechanical and physical performance of natural hydraulic lime mortars. *Constr. Build. Mater.* **290**, 123272 (2021).
40. Baltazar, L. G., Henriques, F. M. & Jorne, F. Optimisation of flow behaviour and stability of superplasticized fresh hydraulic lime grouts through design of experiments. *Constr. Build. Mater.* **35**, 838–845 (2012).
41. Olgun, M. The effects and optimization of additives for expansive clays under freeze–thaw conditions. *Cold Reg. Sci. Technol.* **93**, 36–46 (2013).
42. Yang, J. L., Bai, Y. X., Wang, L. G. & Bai, S. Z. Study on variation and mechanism of mechanical properties of hydraulic lime at different curing age. *J. Exp. Mech.* **37**, 419–429 (2022).
43. Shang, D. J. et al. Influencing factors of chromaticity detection on the reinforced surface of rammed support roof for soil sites. *J. Northwest Norm. Univ. (Nat. Sci.).* **60**, 125–134 (2024).
44. Zhang, J. F. Discussion on color difference by chemical consolidation on earthen sites. *China Cultural Herit. Sci. Res.* **04**, 51–57 (2016).
45. Wei, B., Zhang, Y. M. & Bao, S. X. Effect of calcination conduction on activity of Kaolin and property of geopolymer. *Non-Metallic Mines.* **39**, 31–34 (2016).
46. Tironi, A., Mónica, A. T., Scian, A. N. & Irassar, E. F. Kaolinitic calcined clays: factors affecting its performance as pozzolans. *Constr. Build. Mater.* **28**, 276–281 (2012).

Acknowledgements

This study was funded by the Cultural Relics Science and Technology Research Project of National Cultural Heritage Administration of China (No. 2023ZCK019) and Key Scientific Research Base of Urban Archaeology and Heritage Conservation, State Administration of Cultural Heritage (No. 2023HNKGKY09) and Guangxi Key Technologies R&D Program (No. AB22080102). The funder played no role in study design, data collection, analysis and interpretation of data, or the writing of this manuscript.

Author contributions

Chenhui Liu wrote the main manuscript text. Haitao Yan, Yanhong Li and Yaxin Zhu contributed to the acquisition, analysis, or interpretation of data. Hongbin Zhang participated in the review of the content and quality of the manuscript. All authors read and approved the final manuscript.

Competing interests

The authors declare no competing interests.

Additional information

Correspondence and requests for materials should be addressed to Haitao Yan.